J. Fluid Mech. (2005), *vol.* 544, *pp.* 53–68.
doi:10.1017/S0022112005006579 Printed in the United Kingdom

Stability of vortices in equilibrium with a cylinder

By ALAN R. ELCRAT[1], BENGT FORNBERG[2] AND KENNETH G. MILLER[1]

[1]Department of Mathematics, Wichita State University, Wichita, KS 67260, USA

[2]Department of Applied Mathematics, University of Colorado, Boulder, CO 80309, USA

(Received 4 January 2005 and in revised form 26 May 2005)

The stability of steady inviscid vortex pairs in equilibrium with a circular cylinder is studied by discretizing equations derived from contour dynamics. There are two families of vortices, one with a pair of counter-rotating vortices standing behind the cylinder, which may be thought of as desingularizing the Föppl point vortices, and the other with the vortices standing directly above and below the cylinder. Vortices in the first family are found to be neutrally stable with respect to symmetric perturbations. When asymmetric perturbations are included, there is a single unstable mode and a single asymptotically stable mode. Vortices above and below the cylinder have two modes of instability, one symmetric and the other asymmetric, and likewise two asymptotically stable modes.

1. Introduction

In a previous work (Elcrat *et al.* 2000), we have investigated the variety of possible steady vortex patch equilibria in the symmetric inviscid flows past a circular cylinder. These vortices were organized in terms of families of point-vortex solutions in the same geometry. Starting from any point vortex, a family of vortex patches with the same circulation and expanding areas was obtained. It is natural to consider the stability of these vortices with respect to two-dimensional perturbations. This work is concerned with an investigation of this question.

In this previous work we obtained vortices using an iteration for solutions of the partial differential equation

$$\Delta\psi = f(\psi) \tag{1.1}$$

for the stream function ψ in the special case $f = \omega F(\psi - \alpha)$, $F = 1 - H$, where H is the Heaviside function and α and $\omega > 0$ are constants. This corresponds to a constant vorticity $-\omega$ in the region where $\psi < \alpha$, and irrotational flow elsewhere. The iteration is of the form

$$\Delta\psi_{n+1} = \omega_n F(\psi_n - \alpha), \tag{1.2}$$

where ω_n is chosen so that the area of the vortex,

$$A = |\{\psi_n < \alpha\}|,$$

is a fixed prescribed value. The new proposed vortex is then obtained as a level set of a solution of Poisson's equation, and beyond that, no *a priori* restriction is placed on the vortex boundary. This iterative procedure converges for fairly general initial guesses (we need not start near a solution to obtain convergence), which is part of the appeal of the method. On the other hand there is a limit on the accuracy which can

be obtained with the discretizations used and it is not obvious how to formulate the stability problem using this approach. For this reason we have chosen to reformulate the problem in this paper using a boundary-integral method related to contour dynamics, as has been done by many previous workers (e.g. Zabusky, Hughes & Roberts 1979; Pullin 1981; Wu, Overman & Zabusky 1984; Baker 1990). Solutions obtained by our previous method are used as initial guesses in Newton iterations for these new equations. In this way we obtain highly accurate solutions and stability can be investigated in terms of the eigenvalues of the Jacobian matrix evaluated at the converged solution.

The continuous boundary-integral equations are given in terms of integrals of the appropriate Green's function over the vortex support, and these can be transformed using Green's theorem into contour integrals. Steady flow implies no normal component of velocity and this provides a condition on the contour bounding the vortex which is the basis for our work.

We have used two discretizations to obtain a finite set of equations to solve using Newton's method. In the first, less accurate, discretization we have replaced the contour by a finite set of points, used interpolation of three neighbouring points by a circle to get normal vectors, used the trapezoid rule for the integrals and computed the Jacobian using numerical differentiation. This method converges rapidly for a modest number of points and has the virtue of simplicity. We have used this method to explore various vortex configurations. Unfortunately, this method has difficulty resolving the spectrum of the converged Jacobian so we have used a more accurate method for that purpose. The analysis is more detailed, but allows for analytic computation of the Jacobian. This method also uses Fourier analysis to interpolate the points on the contour for more accurate computation of the integrals.

The stability of these vortices has applications to reduced order models for flow control (see Tang & Aubry 1997; Protas 2004).

In § 2, we derive the boundary-integral formulation of the vortex problem. In § 3, we describe the two discretization methods. In § 4, we give results, and summarize conclusions in § 5.

2. Boundary-integral formulation

In this section we establish notation and derive the equations for vortex equilibrium that we use. It is convenient to employ complex notation and the complex partial derivatives $\partial/\partial z = (\partial/\partial x - \mathrm{i}\partial/\partial y)/2$ and $\partial/\partial \bar{z} = (\partial/\partial x + \mathrm{i}\partial/\partial y)/2$. Some of the calculations that follow are facilitated by noting that if h is a harmonic function, then $\partial h/\partial z = (1/2\mathrm{i})(\mathrm{d}\tilde{h}/\mathrm{d}z)$ where $\tilde{h}$ is the complex analytic function such that $\mathrm{Im}\ \tilde{h} = h$. (We will be dealing with simply connected domains and the disposable real constant will not play a role.)

If ψ is the streamfunction of an incompressible flow with velocity v, $v = \partial\psi/\partial y - \mathrm{i}\partial\psi/\partial x$, then $-\Delta\psi$ is the vorticity. (We identify the two-dimensional vector $\boldsymbol{v} = v_1\boldsymbol{i} + v_2\boldsymbol{j}$ with the complex number $v = v_1 + v_2\mathrm{i}$.) The flow domain Ω is the exterior of the unit disk. In our problem, the vorticity will be a constant ω in a simply connected region D_1 in the upper half-plane, $-\omega$ in a simply connected region D_2 in the lower half-plane, and zero elsewhere in Ω. (All known steady vortex flows past a cylinder are symmetric, i.e. D_2 is the reflection of D_1 across the real axis. However, we include the consideration of asymmetric perturbations, i.e. perturbations for which D_2 is not necessarily the reflection of D_1 across the real axis.) Assuming uniform velocity 1 at

infinity, the streamfunction ψ is given by

$$\psi(z) = \omega \int\int_{D_1} g(z, w)\, \mathrm{d}w_1\, \mathrm{d}w_2 - \omega \int\int_{D_2} g(z, w)\, \mathrm{d}w_1\, \mathrm{d}w_2 + \psi_0(z),$$

where g is the Green's function for $-\Delta$ on Ω, $w = w_1 + \mathrm{i}w_2$ and $\psi_0(z) = \mathrm{Im}(z + 1/z)$ is the streamfunction for potential flow in Ω, uniform at infinity. For the domain Ω, the Green's function g is given explicitly by:

$$2\pi g(z, w) = \log|z - w| - \log|z - 1/\bar{w}|.$$

Since $\bar{v} = 2\mathrm{i}\partial\psi/\partial z$, it follows that

$$\bar{v} = \frac{\omega}{2\pi\mathrm{i}}\left(\int\int_{D_1} \left(-\frac{1}{z - w} + \frac{1}{z - 1/\bar{w}} \right) \mathrm{d}w_1\, \mathrm{d}w_2 + \int\int_{D_2} \left(\frac{1}{z - w} - \frac{1}{z - 1/\bar{w}} \right) \mathrm{d}w_1\, \mathrm{d}w_2 \right) + (1 - z^{-2}).$$

Using the complex form of Green's theorem:

$$\int\int_D \frac{\partial F}{\partial \bar{w}}\, \mathrm{d}w_1\, \mathrm{d}w_2 = -\tfrac{1}{2}\mathrm{i} \oint_C F(w)\, \mathrm{d}w,$$

where C is the boundary of D and, noting that

$$\frac{\partial}{\partial \bar{w}} \left(\frac{\bar{w}}{z} + \frac{1}{z^2} \log\left(\bar{w} - \frac{1}{z} \right) \right) = \frac{1}{z - 1/\bar{w}},$$

we obtain

$$\bar{v}(z) = \frac{\omega}{4\pi} \oint_{\partial D} \left[\log(z - w)\, \mathrm{d}\bar{w} - \left(\frac{\bar{w}}{z} + \frac{1}{z^2} \log\left(\bar{w} - \frac{1}{z} \right) \right) \mathrm{d}w \right] + (1 - 1/z^2), \quad (2.1)$$

where ∂D is the union of ∂D_1 oriented counterclockwise and ∂D_2 oriented clockwise. If D_2 is the reflection of D_1 in the real axis, then this becomes

$$\bar{v}(z) = \frac{\omega}{4\pi} I + (1 - 1/z^2), \quad (2.2)$$

where

$$I = \oint_C \left[\log(z - w)\, \mathrm{d}\bar{w} + \log(z - \bar{w})\, \mathrm{d}w - \frac{1}{z^2} \log\left(w - \frac{1}{z} \right) \mathrm{d}\bar{w} - \frac{1}{z^2} \log\left(\bar{w} - \frac{1}{z} \right) \mathrm{d}w \right], \quad (2.3)$$

with $C = \partial D_1$. We will use this latter formula when considering symmetric perturbations of symmetric flows. In both (2.1) and (2.3), the first term is the only term with a singularity. Following (Pullin 1981), we integrate that term by parts,

$$\oint_C \log(z - w)\, \mathrm{d}\bar{w} = -\oint_C \frac{\bar{z} - \bar{w}}{z - w}\, \mathrm{d}w, \quad (2.4)$$

to obtain an integral with a removable singularity. The formula for $\bar{v}$ resulting from replacing the first term in (2.1) or (2.3) by the right-hand side of (2.4) is what we will use in our analysis.

The contour dynamics of a vortex patch (or pair of vortex patches) with boundary $C(t)$ are given by

$$\frac{\mathrm{d}z}{\mathrm{d}t} = v \quad \text{on} \quad C,$$

where $z = z(s, t)$ is a Lagrangian parameterization of C and the velocity v on C is given by (2.2) when considering only symmetric perturbations, or by (2.1) when considering general perturbations. The flow is stationary if

$$\boldsymbol{v} \cdot \boldsymbol{n} = 0 \quad \text{on} \quad C, \tag{2.5}$$

where $\boldsymbol{n}$ is the unit outward normal to C. We may think of a dynamical system in which marker points on C are given a velocity equal to $(\boldsymbol{v} \cdot \boldsymbol{n})\boldsymbol{n}$. Stationary flows are equilibrium solutions of this dynamical system. Note that (2.1) gives the velocity field on the boundary C as a function of the points on the boundary. Discretizing the integral in (2.1) or (2.3) at N points and imposing (2.5) at the same points gives an autonomous N-dimensional system. We investigate stability by studying the eigenvalues and eigenvectors of the Jacobians of such discretized systems. In this way we can determine whether normal perturbations grow. Details of the discretization procedures are given in the next section.

3. Discretization

We concentrate first on the symmetric problem. The equations which we solve numerically are obtained by discretizing the boundary C of the vortex patch and then requiring $\boldsymbol{v} \cdot \boldsymbol{n} = 0$ at each of the discretization points. Since the velocity is given by (2.3), this requires approximation of the integrals in (2.3) and of the normal direction of C.

Our first discretization uses the trapezoid rule for integrating between the discrete points defining our approximation to C and approximates the normal by the normal to a circle passing through the point and its adjacent discretization points. We solve the resulting system of equations using Newton's method with the partial derivatives in the Jacobian matrix approximated by first-order forward differences. For this discrete Newton's method to converge we must have a good initial guess. Details of how these initial guesses are obtained will be given in the section on results, but here two important points should be made. First, the discrete points on the vortex boundary are merely marker points and the movement of these points should not be confused with the motion of fluid particles in the dynamics of the fluid flow for a curve close to an equilibrium configuration. Secondly, our iteration does not fix area and, for fixed ω, there is always a nearby solution with a slightly different area A and circulation $\kappa = \omega A$. This is reflected in an eigenvalue of the discrete Jacobian which is very close to zero. We have dealt with the problem of the zero eigenvalue by projecting out the smallest singular value of the Jacobian in the initial iterations. More precisely, suppose $\boldsymbol{J}$ is the current Jacobian, and the singular-value decomposition of $\boldsymbol{J}$ is $\boldsymbol{USV}'$: $\boldsymbol{U}$ and $\boldsymbol{V}$ are orthogonal matrices and $\boldsymbol{S}$ is diagonal with the singular values of $\boldsymbol{J}$, in decreasing order, on the diagonal. The situation that we must deal with is that in which the last element of $\boldsymbol{S}$ is nearly zero and the others are orders of magnitude larger. We form the matrix $\boldsymbol{VDU}'$ where $\boldsymbol{D}$ is the diagonal matrix with entries that are the reciprocals of the singular values of $\boldsymbol{J}$, except for the last entry which is 0. We use this matrix in place of the inverse of $\boldsymbol{J}$ in the Newton type iteration. After reaching a sufficiently small successive iteration change we return to the full Newton method. In this way, with a good enough initial guess, we are able to obtain full machine precision in the solution of the discrete equations. We have also used this procedure in the Newton method for the more refined method described next. Also since there is one zero eigenvalue and the remaining eigenvalues occur in conjugate pairs, it is natural to use an odd number N of discretization points.

To obtain greater accuracy in the stability analysis, our second procedure uses analytic expressions for the Jacobian of the discretized system, which we now describe. We consider normal variations $z = z^0 + rn^0$, of a fixed simple closed curve C^0 (an initial guess for the boundary of the desired stationary vortex). Here, z^0 is a parameterization of C^0, n^0 is the unit outward normal and $r = r(s)$ is a real variable. In the discretization, the initial guess C^0 is given as a discretization vector $\boldsymbol{z^0} = (z_1^0, \ldots, z_N^0)$. (We have used discretization points z_j^0 which are equally spaced in terms of chordal arclength. We have not experimented with adapting the parameterization of the current vortex boundary in terms of its geometry, in particular using more points in high-curvature regions. As noted by one of the referees, this would certainly lead to greater efficiency in computing solutions.) Numerical differentiation of the curve gives approximate tangent vectors, and normal directions can be obtained by rotating through 90°; i.e. expressed as complex quantities, the unit normals can be approximated by

$$\boldsymbol{n^0} = -\mathrm{i}\boldsymbol{D z^0}/|\boldsymbol{D z^0}|.$$

Here, $\boldsymbol{D}$ is an $N \times N$ discrete differentiation matrix. We have taken $\boldsymbol{D}$ to be a differentiation matrix based on either fourth-order finite differences or the discrete Fourier transform (Fornberg 1998; Trefethen 2000). For $\boldsymbol{r} = (r_1, \ldots, r_N)^T$ sufficiently small, $\boldsymbol{z} = \boldsymbol{z^0} + \boldsymbol{r n^0}$, will determine a new simple closed curve C. (Here $\boldsymbol{r n^0}$ is the vector obtained by elementwise multiplication). The unit normals to C will likewise be approximated by

$$\boldsymbol{n} = -\mathrm{i}\boldsymbol{D z}/|\boldsymbol{D z}|. \tag{3.1}$$

We discretize the integrals in (2.3) using the trapezoid rule, parameterizing over the interval $[0, 2\pi]$, replacing $\mathrm{d}w$ by $h\,\mathrm{d}w/\mathrm{d}s$ with $h = 2\pi/N$, and approximating $\mathrm{d}w/\mathrm{d}s$ by discrete differentiation: $\mathrm{d}w/\mathrm{d}s = \boldsymbol{D}(\boldsymbol{z^0} + \boldsymbol{r n^0})$. For notational convenience, we let $\boldsymbol{u} = \boldsymbol{D z} = \boldsymbol{D}(\boldsymbol{z^0} + \boldsymbol{r n^0})$. Discretization of (2.2) and (2.3) can then be written

$$\bar{\boldsymbol{v}} = \frac{\omega}{2N}(\boldsymbol{A u} + \boldsymbol{B u} + \boldsymbol{B}_1\bar{\boldsymbol{u}} + \boldsymbol{B}_2\boldsymbol{u}) + (\boldsymbol{1} - \boldsymbol{z}^{-2}), \tag{3.2}$$

where $\boldsymbol{A}, \boldsymbol{B}, \boldsymbol{B}_1$ and $\boldsymbol{B}_2$ are matrices corresponding to the four terms in the integral in (2.3), the first term being replaced by the right-hand side of (2.4). Note that these matrices, as well as the vectors $\bar{\boldsymbol{v}} = (\bar{v}_1, \ldots, \bar{v}_N)^T$, $\boldsymbol{u} = (u_1 \ldots, u_N)^T$ and $\boldsymbol{z}^{-2} = (z_1^{-2}, \ldots, z_N^{-2})^T$, all depend on the independent variable $\boldsymbol{r} = (r_1, \ldots, r_N)^T$.

We next obtain explicit formulae for the matrix with terms $\partial\bar{v}_j/\partial r_k$, $\bar{\boldsymbol{v}}$ given by (3.2). The term $\boldsymbol{Au}$ will be dealt with last. The matrix $\boldsymbol{B}$ has terms $b_{jk} = \log(z_j - \bar{z}_k)$. Note that $\partial b_{jk}/\partial r_i = 0$ except when $i = j$ or $i = k$. This implies that

$$\frac{\mathrm{d}\boldsymbol{B}}{\mathrm{d}\boldsymbol{r}}\boldsymbol{u} = \boldsymbol{B}'\,\mathrm{diag}(\boldsymbol{u}) + \mathrm{diag}(\boldsymbol{B}''\boldsymbol{u}),$$

where $\mathrm{diag}(\boldsymbol{u})$ is the matrix with vector $\boldsymbol{u}$ on the main diagonal, zero elsewhere, $\boldsymbol{B}'$ is the matrix with terms $\partial b_{jk}/\partial r_k$ and $\boldsymbol{B}''$ is the matrix with terms $\partial b_{jk}/\partial r_j$. From the definition of $\boldsymbol{u}$, $\mathrm{d}\boldsymbol{u}/\mathrm{d}\boldsymbol{r} = \boldsymbol{D}\,\mathrm{diag}(\boldsymbol{n^0})$, so we can obtain the matrix $\mathrm{d}(\boldsymbol{Bu})/\mathrm{d}\boldsymbol{r} = (\mathrm{d}\boldsymbol{B}/\mathrm{d}\boldsymbol{r})\boldsymbol{u} + \boldsymbol{B}\mathrm{d}\boldsymbol{u}/\mathrm{d}\boldsymbol{r}$ explicitly. The same remarks apply to the determination of $\mathrm{d}(\boldsymbol{B}_1\bar{\boldsymbol{u}})/\mathrm{d}\boldsymbol{r}$ and $\mathrm{d}(\boldsymbol{B}_2\boldsymbol{u})/\mathrm{d}\boldsymbol{r}$. Turning to $\mathrm{d}(\boldsymbol{Au})/\mathrm{d}\boldsymbol{r}$, there is a singularity in the integrand on the right-hand side of (2.4) when $w = z$; however, it is removable with limit $(\mathrm{d}\bar{z}/\mathrm{d}s)/(\mathrm{d}z/\mathrm{d}s)$, as w approaches z. Since in the discretization $\mathrm{d}z/\mathrm{d}s$ is replaced by the vector $\boldsymbol{u} = \boldsymbol{D}(\boldsymbol{z^0} + \boldsymbol{r n^0})$, we find that the matrix $\boldsymbol{A}$ has terms $a_{jk} = -(\bar{z}_j - \bar{z}_k)/(z_j - z_k)$ for $j \neq k$, $a_{jj} = -\bar{u}_j/u_j$. We then obtain $\mathrm{d}(\boldsymbol{Au})/\mathrm{d}\boldsymbol{r}$ explicitly by the method described above for $\boldsymbol{B}$.

We can now obtain the Jacobian of the discretization of the system (2.5) analytically as a function of $\boldsymbol{r}$. The objective function in (2.5) can be given by $\boldsymbol{F} = \mathrm{Re}(\bar{\boldsymbol{v}}\boldsymbol{n})$ (again the elementwise product of discretization vector components) where $\boldsymbol{v}$ and $\boldsymbol{n}$ are given explicitly by (3.2) and (3.1), respectively. Therefore,

$$\frac{\partial F_j}{\partial r_k} = \mathrm{Re}\left(n_j \frac{\partial \bar{v}_j}{\partial r_k}\right) + \mathrm{Re}\left(\bar{v}_j \frac{\partial n_j}{\partial r_k}\right). \tag{3.3}$$

The computation of $\partial \bar{v}_j / \partial r_k$ is described in the previous paragraph, and by direct differentiation of (3.1)

$$\frac{\partial n_j}{\partial r_k} = -\mathrm{i}\frac{1}{|u_j|}\frac{\partial u_j}{\partial r_k} + n_j \ \mathrm{Re}\left(\frac{i\bar{n}_j}{|u_j|}\frac{\partial u_j}{\partial r_k}\right),$$

where $\partial u_j / \partial r_k = d_{jk} n_k^0$ with d_{jk} the terms of the differentiation matrix $\boldsymbol{D}$.

We have found that for accurate calculation of the eigenvalues, it is useful to write $r = r(\theta)$ as a finite Fourier series

$$r(\theta) = a_0/2 + \sum_{1}^{(N-1)/2} (a_n \cos(n\theta) + b_n \sin(n\theta)), \tag{3.4}$$

where the number N of discretization points is odd. (Here, θ has no direct geometric meaning other than a periodic parameterization of the curve). The vector $\boldsymbol{c} = (a_0, a_1, \ldots, a_{(N-1)/2}, b_1, \ldots, b_{(N-1)/2})^T$ of Fourier coefficients can be obtained from $\boldsymbol{r} = (r_1, \ldots, r_N)^T$ by multiplying $\boldsymbol{r}$ on the left-hand side by a fixed square matrix $\boldsymbol{M}_1$. We can use the finite Fourier series to interpolate $\boldsymbol{r}$ at $Q = kN$ quadrature points for the discretization of the integrals in (2.3) and (2.4). Here k is an even number, typically 2 or 4. The vector $\tilde{\boldsymbol{r}} = (\tilde{r}_1, \ldots, \tilde{r}_Q)^T$ of interpolated quadrature points can be obtained from $\boldsymbol{c}$ by multiplying $\boldsymbol{c}$ on the left-hand side by a fixed $Q \times N$ matrix $\boldsymbol{M}_2$. This results in a slight modification of the previous four paragraphs: $\boldsymbol{D}$ is now a $Q \times Q$ differentiation matrix, $\boldsymbol{z} = \boldsymbol{z}^0 + \tilde{\boldsymbol{r}}\boldsymbol{n}^0$ and $\boldsymbol{u} = \boldsymbol{D}\boldsymbol{z}$ are length Q vectors, and the matrices $\boldsymbol{A}, \boldsymbol{B}, \boldsymbol{B}_1$ and $\boldsymbol{B}_2$ in (3.2) are $N \times Q$ matrices. We use the Fourier coefficients $\boldsymbol{c}$ as variables in solving the N equations $\boldsymbol{F} = 0$ by Newton's method. The Jacobian matrix needed for Newton's method can be found analytically

$$\frac{\mathrm{d}\boldsymbol{F}}{\mathrm{d}\boldsymbol{c}} = \frac{\mathrm{d}\boldsymbol{F}}{\mathrm{d}\tilde{\boldsymbol{r}}}\frac{\mathrm{d}\tilde{\boldsymbol{r}}}{\mathrm{d}\boldsymbol{c}} \quad \text{where} \quad \frac{\mathrm{d}\tilde{\boldsymbol{r}}}{\mathrm{d}\boldsymbol{c}} = \boldsymbol{M}_2 \tag{3.5}$$

and $\mathrm{d}\boldsymbol{F}/\mathrm{d}\tilde{\boldsymbol{r}}$ is the $N \times Q$ matrix with terms given by (3.3) (with r_k replaced by $\tilde{r}_k$).

We have used analytic Jacobian formulae both to obtain highly accurate stationary vortices by starting from a fairly good guess C^0 and also to do the stability analysis when C is an accurate solution. We point out that in doing the stability analysis for an accurate solution C, we cannot use the Jacobian (3.3) from the final step in the Newton iteration used to obtain C from an initial guess. The reason is that the vectors $\boldsymbol{n}^0$ determining the coordinate system are not necessarily normal to C. We must recompute using the above analysis with $\boldsymbol{z}^0$ a discretization of C and $\boldsymbol{r} = 0$. The matrix $\mathrm{d}\boldsymbol{F}/\mathrm{d}\boldsymbol{r}$ required for the stability analysis is then obtained by multiplying $\mathrm{d}\boldsymbol{F}/\mathrm{d}\boldsymbol{c}$ given by (3.5) on the right-hand side by $\mathrm{d}\boldsymbol{c}/\mathrm{d}\boldsymbol{r} = \boldsymbol{M}_1$.

To consider asymmetric perturbations we assign separate variables to a discretization of C and a discretization of its reflection $\bar{C}$ in the real axis. There is a slight modification to the above analysis based on using (2.1) rather than (2.2).

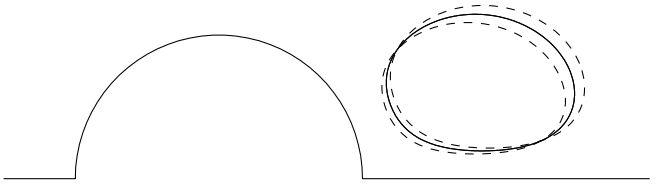

FIGURE 1. Detached stationary vortex behind a cylinder and perturbations (dashed curves) of the vortex boundary in the directions (+ and −) of the eigenvector for eigenvalue 0. Perturbations in the direction of this eigenvector lead to additional solutions with the same ω (see figure 10).

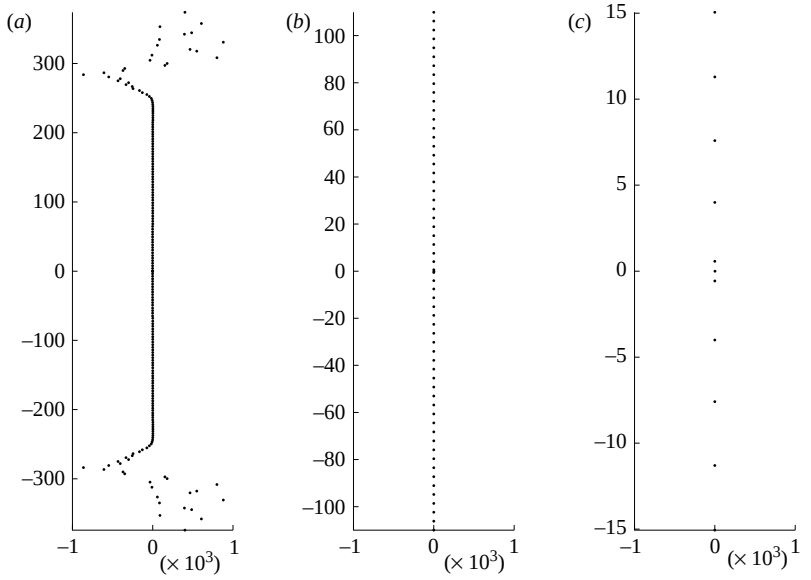

FIGURE 2. Eigenvalues for the vortex in figure 1. (*a*) All the eigenvalues at a particular level of discretization. (*b*, *c*) Enlargements of this plot; (*b*) shows the near equal spacing on the imaginary axis, except for the first conjugate pair which is closer to 0, as seen in (*c*).

4. Results

We first present results for a detached vortex either behind or above a semicircle in the upper half-plane. Stability results for perturbations of the half-plane flow imply corresponding results for *symmetric* perturbations of the symmetric flow past a cylinder obtained by reflection in the x-axis. Near the end of the section, we consider asymmetric perturbations to symmetric flow past the cylinder.

To set the tone for our results, we first consider a specific vortex behind the semicircle, that with circulation $\kappa = 8$ and $\omega = 8$, plotted in figure 1. We have used both methods described above to compute the vortices, but for detailed results on the spectrum of the Jacobian, we have relied on the more accurate method. The computed eigenvalues of $\boldsymbol{J} = \mathrm{d}\boldsymbol{F}/\mathrm{d}\boldsymbol{r}$ for this solution are plotted in figure 2. The results described here were obtained with $N = 201$, but results are persistent when N is changed, as will be discussed more thoroughly near the end of this section. We note that most of the spectrum is concentrated on the imaginary axis. By refinement of the grid, the scatter at the top in figure 2(*a*) is shown to be spurious, owing to discretization. We conclude from this that the vortex is neutrally stable to two-dimensional perturbations.

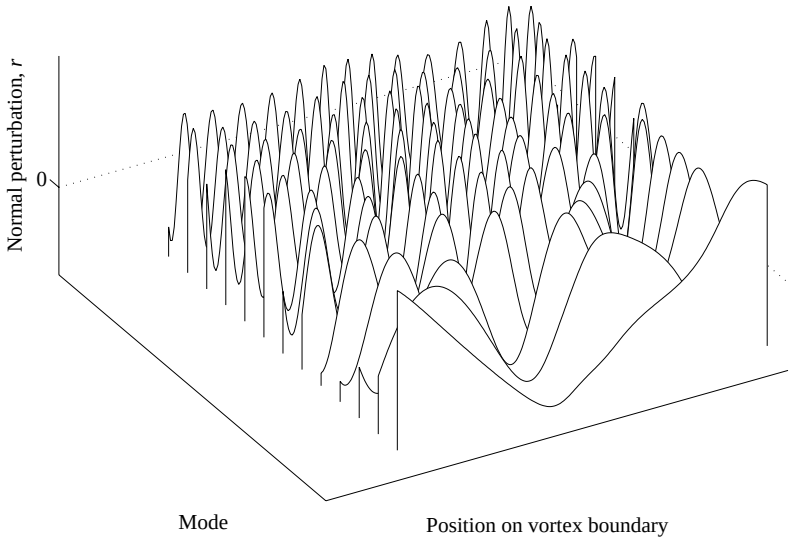

FIGURE 3. Real parts of the eigenvectors for the first 13 non-zero eigenvalues for the vortex in figure 1. Imaginary parts have similar profiles, but with a 'phase shift'.

The eigenvalues are nearly equally spaced on the imaginary axis, except for the gap between the first imaginary pair and zero, which is smaller.

We obtain more information by examining the eigenvectors, which may be considered as functions of the equally spaced discretization points on the boundary of the vortex. As noted earlier, zero is always an eigenvalue. A perturbation of the vortex boundary by an eigenvector corresponding to eigenvalue 0 is shown as a dashed curve in figure 1. A waterfall plot of the real parts of the eigenvectors corresponding to the first several eigenvalues with positive imaginary part is shown in figure 3. It is noted that, except for the first eigenvector, the real parts of the eigenvectors are nearly sinusoidal in shape, with n maxima for the nth eigenvector. The frequency content in all the eigenmodes is exhibited in a waterfall plot of an application of the fast Fourier transform to the eigenvectors (figure 4).

In eigenvector plots such as figures 3 and 5, the eigenvectors have been normalized to have the same Euclidean norm. Superimposing the eigenvectors on a single plot reveals that there is a distinct 'envelope' of the normalized eigenvectors. Figure 5 shows the real and imaginary parts of the eigenvectors for the fourth to the twelfth eigenvalues. Excluding the spurious eigenvalues, eigenvectors corresponding to higher eigenmodes are also within the same envelope. The similarity in the profile of the eigenvector envelope and the fluid pressure in figure 5 indicates that the amplitude of any 'oscillations' of a slight perturbation of the vortex will generally be larger near points where the pressure is larger. Any small local shape disturbance in the vortex will just travel (dispersion and dissipation free) around the boundary, with its amplitude varying with the local pressure. Figure 6 shows perturbations of the vortex boundary in the direction of the real part of the eigenvector corresponding to the first eigenvalue with positive imaginary part.

We next consider a stationary vortex standing above the semicircle. An example is shown in figure 7. For this vortex, there is a single unstable mode with eigenvalue 0.282, as seen in the eigenvalue plot figure 8. A perturbation in the direction of the unstable mode is shown in figure 7(b). Figure 9 shows that again for this vortex,

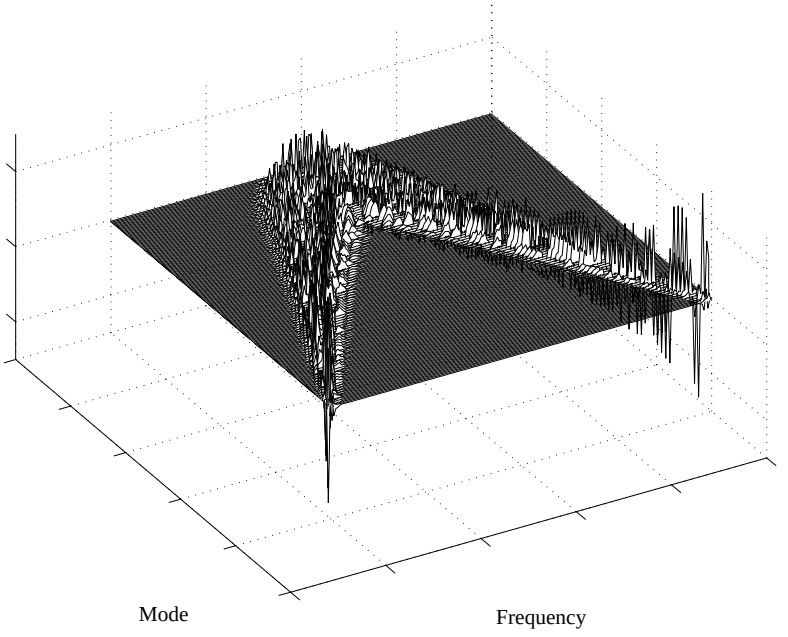

FIGURE 4. Frequency plot for all the eigenmodes of the vortex in figure 1.

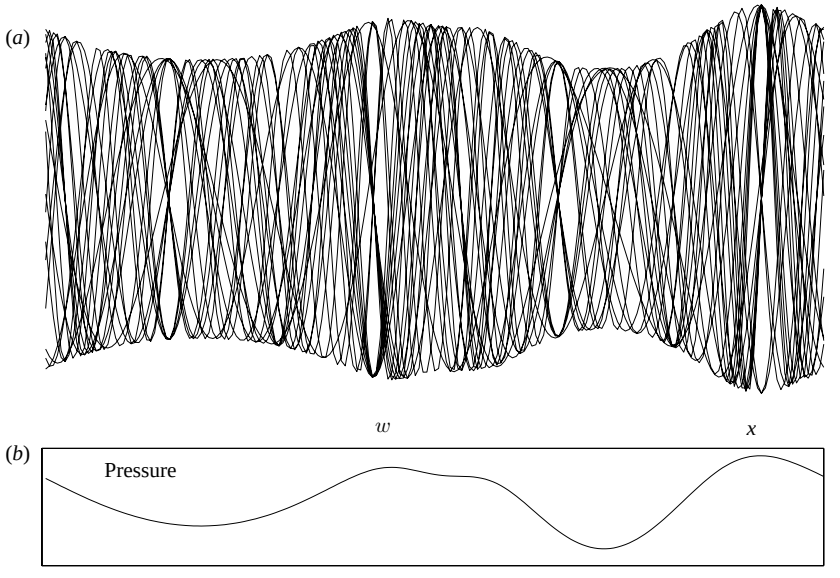

FIGURE 5. (*a*) A plot of several eigenvectors $\boldsymbol{r}(z)$ for the vortex in figure 1, (*b*) the pressure on the vortex boundary. The horizontal axis gives the position along the vortex boundary measured from some reference point. Points w and x of maximum relative pressure are indicated on figure 6.

eigenmodes with non-zero imaginary part lie within a distinct envelope and that this envelope bears a similarity to the pressure profile on the vortex boundary.

In all cases which we have investigated, we have found neutral stability for detached vortices behind the semicircle, and one unstable mode for symmetric vortices above

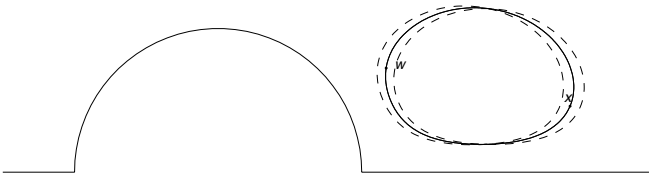

FIGURE 6. Perturbation of a stationary vortex in the direction of the eigenvector for the first purely imaginary eigenvalue. Points w and x on the boundary are where the pressure has a relative maximum. As figure 5 indicates, other eigenmodes also tend to have higher amplitude at these points.

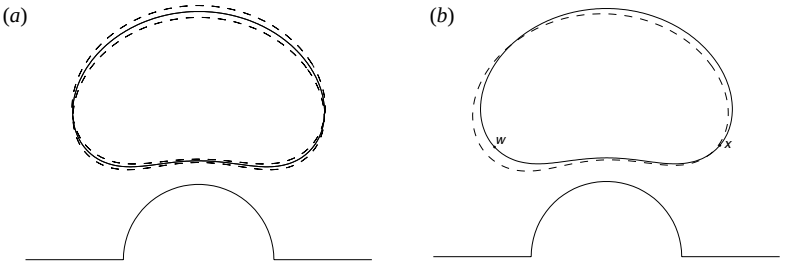

FIGURE 7. A stationary vortex above the cylinder: (a) also shows perturbations in the direction of the zero eigenvector, leading to nearby steady solutions; (b) shows a perturbation in the direction of the single unstable eigenmode. Points w and x are points of maximum pressure (see figure 9).

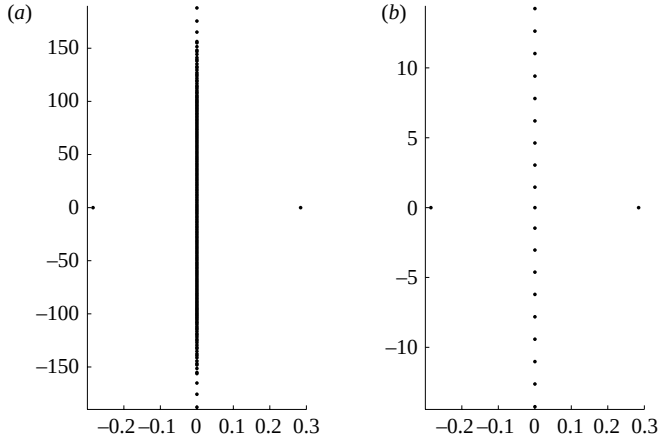

FIGURE 8. Eigenvalues for the vortex in figure 7. There is a single positive eigenvalue. Eigenvalues on the imaginary axis are nearly equally spaced.

the semicircle. This is consistent with the fact that for point vortices, Föppl vortices are stable (as a single vortex in the upper half- plane – the corresponding vortex pair being stable with respect to symmetric perturbations), whereas point vortices on the vertical axis are unstable.

As noted earlier, $\lambda = 0$ is always an eigenvalue, because each vortex is part of a one-parameter family of vortex solutions with the same ω. Perturbation of the vortex boundary in the direction of the eigenfunction corresponding to $\lambda = 0$ will lead to other vortices with the same ω. For the vortex in figure 1, perturbation in the direction

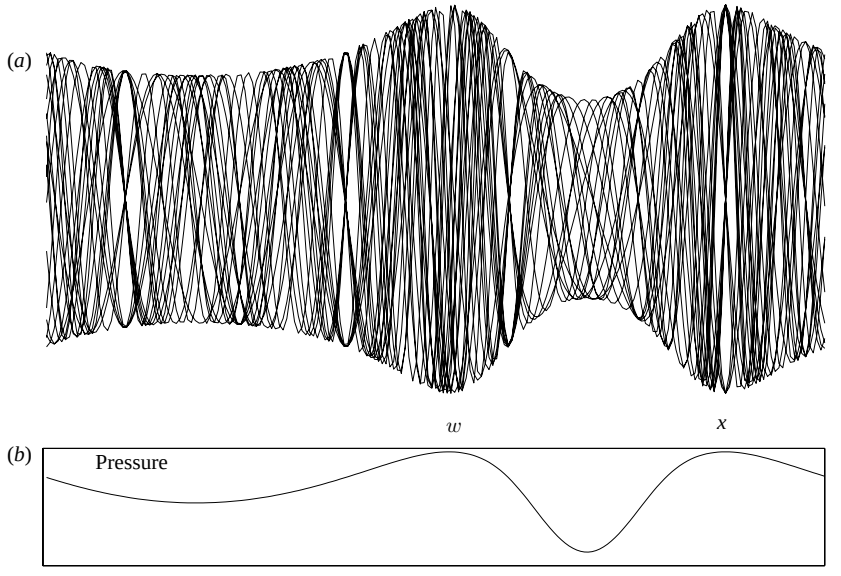

FIGURE 9. Eigenvectors and pressure for the vortex in figure 7. Points w and x of maximum pressure are indicated in figure 7(b).

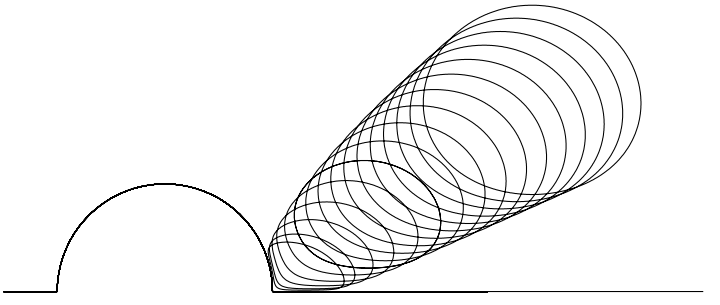

FIGURE 10. A sequence of stationary vortices with ω fixed, obtained by perturbing the vortex in figure 1.

of the zero eigenvector leads to the family of vortices shown in figure 10. Figure 11 shows a similar family beginning with the vortex in figure 7. To obtain these vortices, $\boldsymbol{z} + \delta \boldsymbol{r}\boldsymbol{n}$ was taken as a new initial guess for the algorithm, where $\boldsymbol{z}$ is the previous solution, $\boldsymbol{r}$ is the zero eigenvector for that solution, $\boldsymbol{n}$ gives the unit normals to the curve determined by $\boldsymbol{z}$ and δ is a perturbation parameter, taken to be ± 0.2 in these calculations. Convergence was obtained in two or three Newton iterations. Every tenth solution has been plotted.

We next consider a sequence of vortices all with the same circulation $\kappa = 8$, but with different values of ω, as shown in figure 12. The smallest of these vortices was obtained by taking as initial guess a circle with small radius centred at the Föppl point-vortex location. Subsequent solutions were obtained by normal perturbation, i.e. using $\boldsymbol{z} + \delta \boldsymbol{n}$ as initial guess. For vortices that are nearly circular, the real and imaginary parts of the eigenfunctions are nearly sinusoidal. At the other end of the family, the largest vortex shown in figure 12 is nearly attached. The eigenvalues for this solution are shown in figure 13, and the real parts of the first several eigenvectors are shown in figure 14. The envelope of the real and imaginary parts of the eigenvectors and

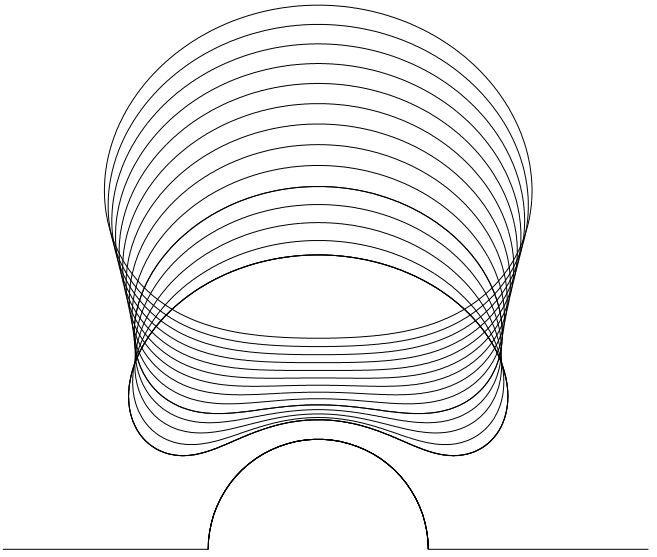

FIGURE 11. A sequence of stationary vortices with ω fixed, obtained by perturbing the vortex in figure 7.

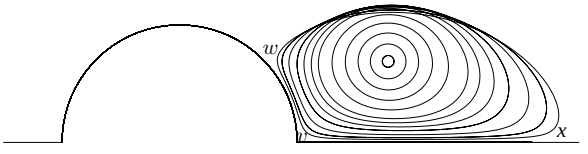

FIGURE 12. A sequence of stationary vortices with the same circulation $\kappa = 8$, all desingularizing the same Föppl point vortex.

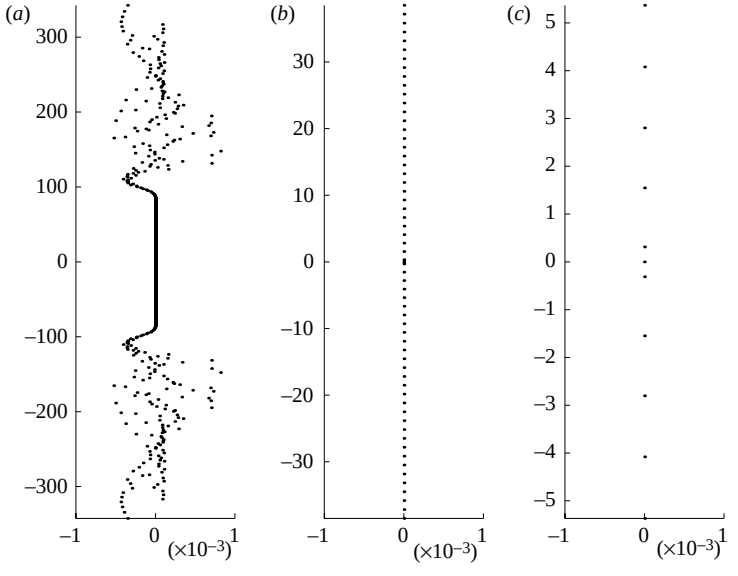

FIGURE 13. Eigenvalues for the nearly attached vortex in figure 12. (*b*) and (*c*) Enlargements of portions of the full eigenvalue plot shown in (*a*).

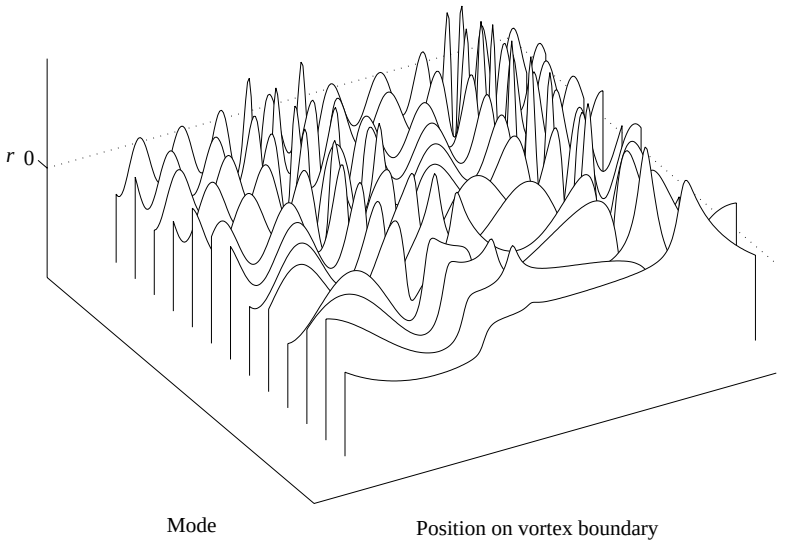

FIGURE 14. Eigenvectors for the first 13 non-zero eigenvalues for the nearly attached vortex in figure 12.

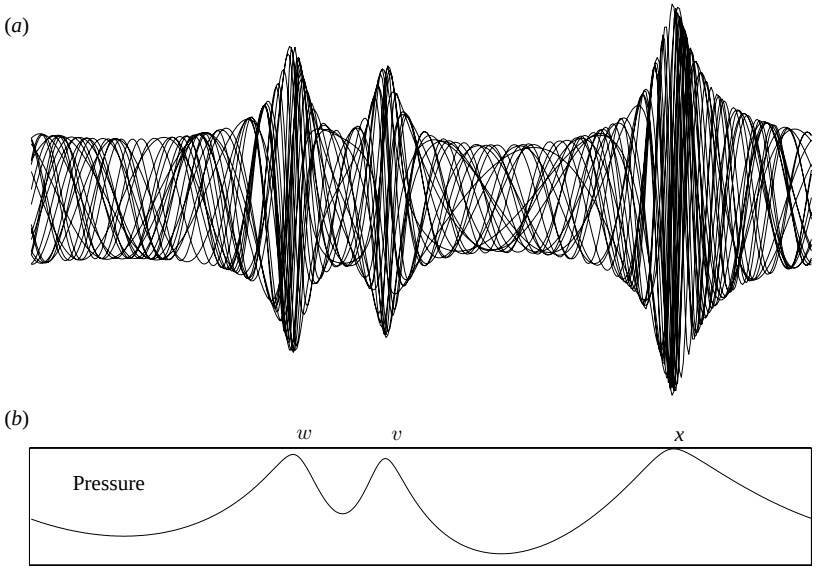

FIGURE 15. Eigenvectors and pressure for the nearly attached vortex in figure 12. The points of maximal pressure are also shown in figure 12.

its similarity to the pressure on the boundary of the vortex are shown in figure 15. For this vortex, the pressure profile is much less uniform than that for the vortex in figure 1. Any small disturbance to the equilibrium state for the vortex boundary will be more strongly concentrated near the points w, v and x shown in figure 12.

Ignoring the scatter far from the real axis, the spacing between successive eigenvalues for a fixed vortex appears to be nearly constant. Except for the distance between 0 and the first eigenvalue $\lambda_1 \mathrm{i}$ on the positive imaginary axis, the gap between successive eigenvalues is very close to $\omega/2$ for vortices close to circular in shape

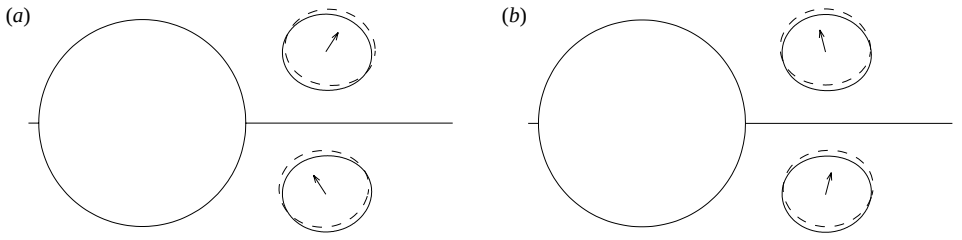

FIGURE 16. (*a*) The unstable mode, and (*b*) the asymptotically stable mode, for a vortex pair when $\kappa = 8$ and the area of each vortex component is 0.5. For sake of comparison, the eigenvectors for the point-vortex system with the same circulation are shown as arrows based at the point-vortex locations. The eigenvalues for the vortex patch solution are ± 0.5266 while the eigenvalues for the point-vortex solution are ± 0.5251.

and is always less than $\omega/2$. When the vortex is a small area desingularization of a Föppl point vortex, $\pm\lambda_1 \mathrm{i}$ is very close to the purely imaginary eigenvalues for the Föppl point-vortex pair with the same circulation. (An analysis of the eigenvalues and eigenvectors for the Föppl point vortex can be found in Tang & Aubry 1997.) The value of λ_1 decreases rather slowly as the area of the vortex is increased and circulation is held fixed. Thus, the first imaginary eigenvalue depends primarily on the circulation κ whereas the gap between successive eigenvalues is related to the vortex strength ω.

The behaviour of attached vortices such as the one being approached in figure 12 is intriguing. For detached vortices, perturbations of shape advect around the boundary; however, there can be no such shape perturbation along the attached part of the boundary. Moreover, the computation of such attached vortices is extremely delicate using contour dynamics equations. We have attempted to approach this problem by studying the related problem of translating vortex pairs, also called translating V-states in Wu *et al.* (1984). These have been computed by Saffman & Tanveer (1982) and Wu *et al.* (1984). This requires modifications of our programs which we have carried out for the simpler method. However, this modification was not adequate for resolving the eigenvalues of the attached pair, and the more accurate method uses periodicity in an essential way. Dritschel (1995) has studied the stability of rotating vortex pairs with respect to general perturbations. The special case of equal area and a translating vortex pair is included in his study, and he has found a rotational instability. He found no evidence of symmetric instability (Dritschel, personal communication).

We now consider symmetric flow past a cylinder and allow independent perturbations of the vortex in the upper half-plane and its reflection in the lower half-plane. For vortices behind the cylinder, there is now one unstable mode and one asymptotically stable mode. For small area desingularizations of a Föppl point-vortex pair, the positive and negative eigenvalues are very close to the two real eigenvalues of the corresponding point-vortex system. (As shown in Tang & Aubry (1997), the point-vortex system has four eigenvalues: one positive, one negative and an imaginary pair). Perturbations of the vortex pair in the direction of these two modes are shown in figure 16. In addition to the symmetric neutrally stable modes obtained previously, there are also asymmetric neutrally stable modes. Denote by $\lambda_k \mathrm{i}$ the kth eigenvalue on the positive imaginary axis for the symmetric problem. Then, for $k \geqslant 2$, there is a λ_k' close to λ_k such that $\pm\lambda_k' \mathrm{i}$ is a second pair of eigenvalues for the asymmetric problem. Perturbations in the directions of the eigenvectors for $\pm\lambda_k' \mathrm{i}$ are not symmetric (see figure 17). As k increases, $\lambda_k - \lambda_k'$ decreases and the

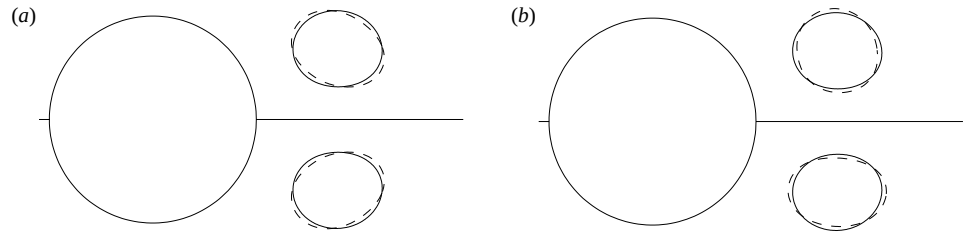

FIGURE 17. Symmetric and asymmetric neutrally stable modes for $k=2$. Eigenvalues for the modes are (*a*) $\pm\lambda_2$i and (*b*) $\pm\lambda_2'$i where $\lambda_2=7.9955$ and $\lambda_2'=7.6667$. In general, the real and imaginary parts of the eigenfunctions for both λ_ki and λ_k'i have k maxima and k minima on each vortex boundary component. For $k=1$, there is no corresponding asymmetric neutral mode.

(*a*)							(*b*)					
N_1	N_2	7 s.f.	6 s.f.	5 s.f.	4 s.f.	3 s.f.	N_1	N_2	6 s.f.	5 s.f.	4 s.f.	3 s.f.
81	161	0	0	2	7	12	81	161	0	0	2	5
161	321	0	4	8	12	21	161	321	0	3	8	18
321	641	3	8	12	21	54	321	641	3	4	18	31

TABLE 1. Persistence of the computed eigenvalues with changes in the number N of discretization points. Entries give the number of eigenvalues with positive imaginary part for which there is agreement to a given number of significant figures (s.f.), when comparing two solutions with different values of N. (*a*) is for the vortex shown in figure 1 – a typical case. (*b*) is for the more extreme case of the nearly attached vortex shown in figure 12.

difference becomes smaller than the accuracy of our calculations at about $k=12$ for the example shown. Zero is a double eigenvalue for the asymmetric problem.

For any flow with vortices directly above and below the cylinder, for example the flow in figure 7 together with its reflection, there is an asymmetric unstable mode in addition to the symmetric unstable mode found earlier. For each of the two positive eigenvalues, its negative is also an eigenvalue, giving two asymptotically stable modes.

We next provide some data indicating the persistence of the computed eigenvalues with changes in the number of discretization points N. For the vortex shown in figure 1, table 1 shows how many eigenvalues agree to a given accuracy when comparing the computations with $N=N_1$ and $N=N_2$. For example, the last entry in the first row of table 1(*a*) indicates that the first 12 eigenvalues on the positive imaginary axis agree to three significant figures. The accuracy decreases monotonically going up the positive imaginary axis. It appears that doubling the number of discretization points increases the accuracy by roughly one order of magnitude. We note that accuracy is diminished for the vortex that is close to attached.

5. Conclusions

For stationary vortex flows past a cylinder with patches of constant vorticity, we have studied stability with respect to both symmetric and asymmetric perturbations. This has been done by formulating equations for normal perturbations based on contour dynamics equations and computing the eigenvalues of Jacobians of discretizations of these equations at a solution. There are two families of vortices, those desingularizing the family of Föppl point vortices behind the cylinder and those

desingularizing point vortices standing above and below the cylinder. The vortices behind the cylinder have been found to have purely imaginary eigenvalues with respect to symmetric perturbations and, like the Föppl point vortices, a single mode of instablity with respect to asymmetric perturbations. This extends up to vortices which are almost attached.

Vortices in the family directly above and below the cylinder have exactly two unstable modes, one symmetric and one asymmetric. For any fixed vortex, in either family, the normalized eigenvectors for the imaginary eigenvalues lie in a well-defined envelope which has a profile similar to that of the fluid pressure on the boundary. For these modes, perturbations of the vortex shape advect around the boundary with amplitude varying with the local pressure.

A significant feature of the problems considered is that there is always a nearby solution and this leads to a zero singular value of the Jacobian. We have dealt with this by modifying Newton's method by removing this singular value in a factorization of generalized inverse of the Jacobian. The techniques used here can be used for other vortex configurations and may include asymmetric perturbations. It is also possible to generalize these techniques to axisymmetric problems and we intend to do this in the future and apply this to the flows found in Elcrat, Fornberg & Miller (2001).

B. F. received support from grant NSF-DMS-0309803.

REFERENCES

Baker, G. 1990 A study of the numerical stability of the method of contour dynamics. *Phil. Trans. R. Soc. Lond.* A **333**, 391–400.

Dritschel, D. G. 1995 A general theory for two-dimensional vortex interactions. *J. Fluid Mech.* **293**, 269–303.

Elcrat, A., Fornberg, B., Horn, M. & Miller, K. 2000 Some steady vortex flows past a circular cylinder. *J. Fluid Mech.* **409**, 13–27.

Elcrat, A., Fornberg, B. & Miller, K. 2001 Some steady axisymmetric vortex flows past a sphere. *J. Fluid Mech.* **433**, 315–328.

Fornberg, B. 1998 *A Practical Guide to Pseudospectral Methods*. Cambridge University Press.

Protas, B. 2004 Linear feedback stabilization of laminar vortex shedding based on a point vortex. *Phys. Fluids* **16**, 4473–4488.

Pullin, D. I. 1981 The nonlinear behavior of a constant vorticity layer at a wall. *J. Fluid Mech.* **108**, 401–421.

Saffman, P. G. & Tanveer, S. 1982 The touching pair of equal and opposite uniform vortices. *Phys. Fluids* **25**, 1929–1930.

Tang, S. & Aubry, N. 1997 On the symmetry breaking instability leading to vortex shedding. *Phys. Fluids* **9**, 2550–2561.

Trefethen, L. N. 2000 *Spectral Methods in MATLAB*. SIAM, Philadelphia.

Wu, H. M., Overman, E. A. & Zabusky, N. 1984 Steady-state solutions of the Euler equations in two dimensions: rotating and translating V-states with limiting cases. I. Numerical algorithms and results. *J. Comput. Phys.* **53**, 42–71.

Zabusky, N. J., Hughes, M. H. & Roberts, K. V. 1979 Contour dynamics for the Euler equations in two dimensions. *J. Comput. Phys.* **30**, 96–106.